Coaxial $Ni_xCo_{2x}(OH)_{6x}$/TiN Nanotube Arrays as Supercapacitor Electrodes

Chaoqun Shang,[†,‡,⊥] Shanmu Dong,[†,⊥] Shan Wang,[†,‡] Dongdong Xiao,[§] Pengxian Han,[†] Xiaogang Wang,[†] Lin Gu,[§] and Guanglei Cui[†,*]

[†]Qingdao Institute of Bioenergy and Bioprocess Technology, Chinese Academy of Sciences, Qingdao 266101, People's Republic of China, [‡]University of Chinese Academy of Sciences, Beijing 100049, People's Republic of China, and [§]Institute of Physics, Chinese Academy of Sciences, Beijing 100080, People's Republic of China. [⊥]C. Shang and S. Dong contributed equally to this work.

ABSTRACT $Ni_xCo_{2x}(OH)_{6x}$, as a precursor of intensively studied $NiCo_2O_4$, has been directly deposited into self-standing titanium nitride nanotube array (TiN NTA) grid monolithic supports to form a coaxial nanostructured electrode for supercapacitors. With TiN NTA substrates providing a large surface area, fast electron transport, and enhanced structure stability, this $Ni_xCo_{2x}(OH)_{6x}$/TiN electrode exhibits superior pseudocapacitive performance with a high specific capacitance of 2543 F g^{-1} at 5 mV s^{-1}, remarkable rate performance of 660 F g^{-1} even at 500 mV s^{-1}, and promising cycle performance (about 6.25% capacitance loss for 5000 cycles). Interestingly, the $Ni_xCo_{2x}(OH)_{6x}$/TiN NTA electrode outperforms the $NiCo_2O_4$/TiN NTA electrode, indicating that this self-standing $Ni_xCo_{2x}(OH)_{6x}$/TiN NTA monolith is a promising candidate for high-performance supercapacitor applications.

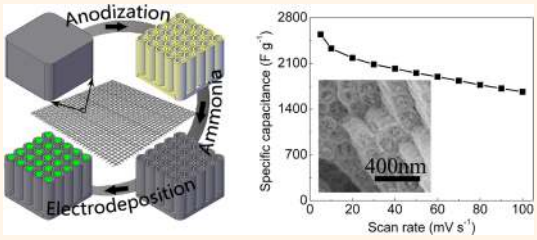

KEYWORDS: $Ni_xCo_{2x}(OH)_{6x}$ · TiN NTA · self-standing electrode · supercapacitors · pseudocapacitive performance

Supercapacitors have attracted tremendous attention because of their high power density and long cycle life.[1−5] For pseudocapacitor applications, transition metal oxides/hydroxides are widely investigated,[6−9] as they can provide multiple oxidation states for reversible Faradaic reactions. In many reports, $Ni(OH)_2$ and $Co(OH)_2$ have been widely explored owing to their abundance, low cost, and environmental benignity.[10−14] $Ni(OH)_2$ possesses high theoretical specific capacitance, but its poor intrinsic conductivity restricts its rate capability.[15−17] On the other hand, $Co(OH)_2$ exhibits much higher conductivity.[18,19] Consequently, the integration of Ni and Co hydroxides always possesses enhanced specific capacitance and rate capability.[16,20−23] Unfortunately, the high rate performance is still unsatisfactory.

To enhance the rate capability of Ni and Co hydroxides, an efficient design is to directly grow the active materials on a nanostructured self-standing current collector.[24,25] This monolithic design has apparent advantages as follows:[26−29] (i) the nanostructure of the current collector serves a large surface area, which would be favorable for active materials accessible to an electrolyte; (ii) a conductive current collector directly attached to active materials provides fast electron transport, which improves the rate capability; (iii) compared to common slurry-coating technology, where a large area of active surface material is blocked by binders, this design would render auxiliary components such as binder and conductive agents and significantly reduce specific energy density and even specific power density. Among various options for self-standing substrates, titanium nitride (TiN), with excellent electronic conductivity, corrosion resistance, and low cost, is an attractive candidate.[30,31] Furthermore, the nanostructured TiN monolithic collector can be a potential choice to enhance the rate capability of Ni and Co hydroxides. However, there are still limited reports on growing Ni and Co hydroxides on a self-standing TiN support.[24]

Herein, based on TiN nanotube arrays (NTA), we report a self-standing strategy to grow a mixed bimetallic hydroxide [denoted as $Ni_xCo_{2x}(OH)_{6x}$], which is always used as a precursor to synthesize $NiCo_2O_4$.[28] $NiCo_2O_4$ has been extensively investigated because of its high electrochemical activity,[32−35] but to our surprise, the pseudocapacitor performance of its precursor does not arouse

* Address correspondence to cuigl@qibebt.ac.cn.

Received for review March 21, 2013 and accepted May 6, 2013.

Published online May 06, 2013
10.1021/nn401402a

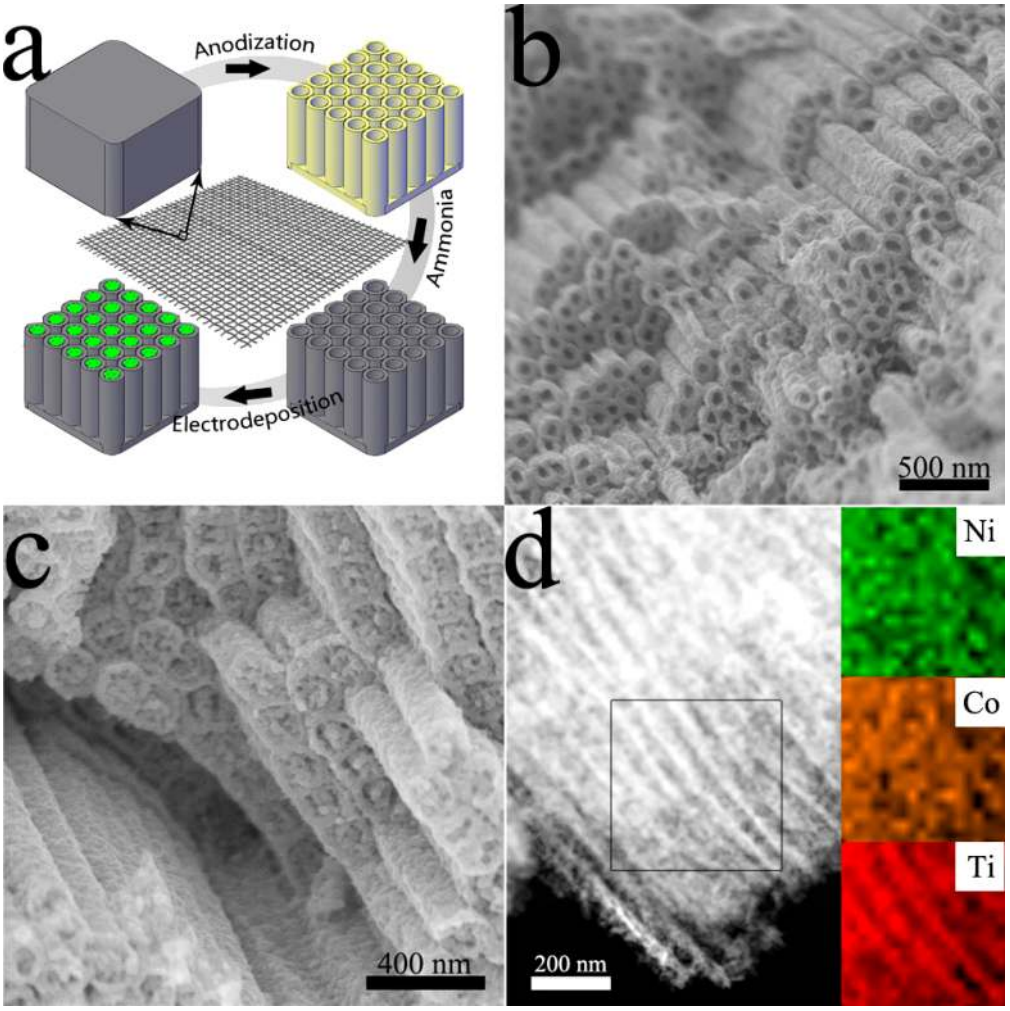

Figure 1. (a) Schematic illustration of $Ni_xCo_{2x}(OH)_{6x}$/TiN NTA preparation. (b) Typical SEM image of a pristine TiN NTA. (c) Typical SEM image of a TiN NTA after deposition of $Ni_xCo_{2x}(OH)_{6x}$. (d) Typical STEM image of $Ni_xCo_{2x}(OH)_{6x}$/TiN NTA.

much attention. In this paper, $Ni_xCo_{2x}(OH)_{6x}$ was directly grown on titanium nitride nanotube arrays (TiN NTA) by co-electrodeposition to obtain a coaxial nanostructure self-standing monolithic electrode with high rate performance. Compared with $NiCo_2O_4$, our findings demonstrate that $Ni_xCo_{2x}(OH)_{6x}$ materials can deliver superior capacity and rate capability.

RESULTS AND DISCUSSION

Synthesis and Structural Analysis. Figure 1a illustrates the process to synthesize $Ni_xCo_{2x}(OH)_{6x}$/TiN NTA including anodization, calcination in ammonia, and electrodeposition. In our previous reports, Ti foil has been involved to fabricate NTA.[36,37] Herein, we chose Ti mesh to prepare TiN NTA (as shown in Figure S1), because Ti mesh has a much larger surface area than Ti foil. Therefore, an improved performance can be expected. After calcination, the obtained pristine TiN NTA possess uniform nanotube arrays with outer diameters in the range 100−120 nm, as shown in Figure 1b. These one-dimensional arrays on a Ti mesh substrate with a fast electron transport network can serve as a favorable current collector. Through optimized electrochemical deposition, the binary Ni−Co hydroxides are deposited in a well-distributed manner into the TiN nanotube (Figure 1c and d) to form coaxial nanowire arrays. Elemental mapping also reveals a uniform distribution of Ni and Co in the TiN NTA (inset of Figure 1d). This nanostructure ensures (i) improved electronic conductivity owing to the contribution of TiN materials, (ii) enhanced ionic conductivity and favorable access to the eletrolyte by avoiding the binder, and (iii) high utilization of well-dispersed active materials on the large surface area of the NTA substrates. Furthermore, the deposited Ni−Co hydroxides inside the NTA are highly porous and form a nanosheet like rippled silk when grown on the TiN film (as shown in Figure S2). This morphology endowed by electrochemical deposition further improves the surface area of the active materials, facilitating charge storage in the double layer.

To demonstrate the ratio of Ni/Co in the as-prepared samples, XRD analysis was conducted. Figure 2a shows the XRD pattern of the as-prepared Ni−Co

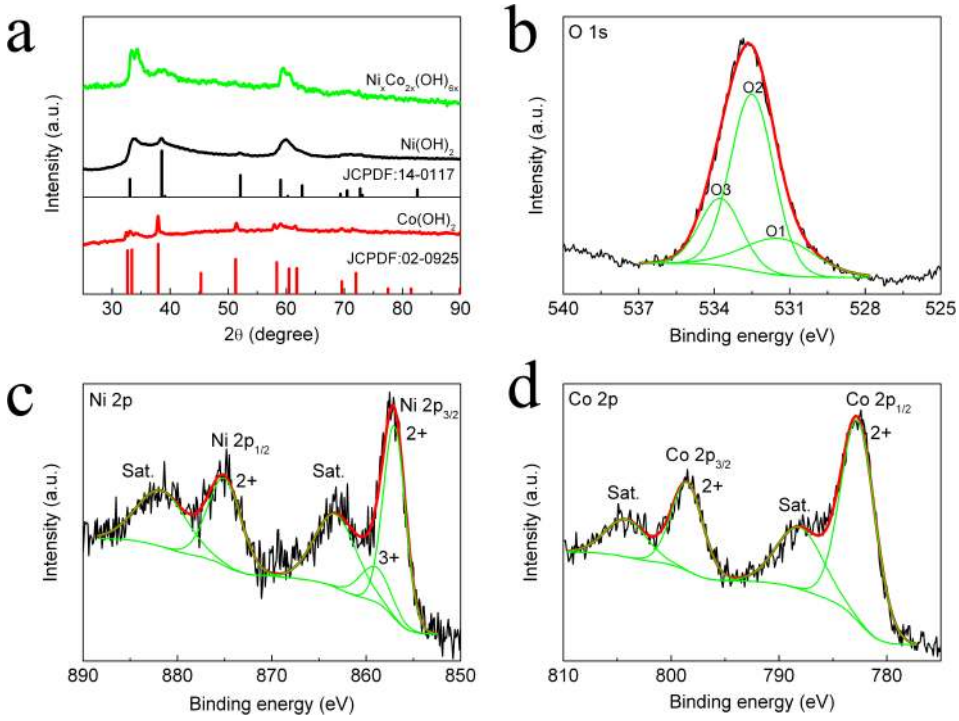

Figure 2. (a) XRD patterns of $Ni_xCo_{2x}(OH)_{6x}$, (b) O 1s XPS, (c) Ni 2p XPS, and (d) Co 2p XPS of $Ni_xCo_{2x}(OH)_{6x}$/TiN NTA.

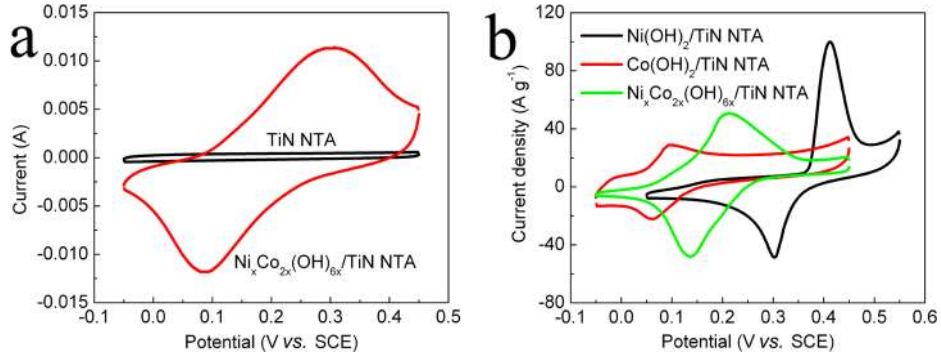

Figure 3. (a) CV curves of TiN NTA and $Ni_xCo_{2x}(OH)_{6x}$/TiN NTA at a scan rate of 100 mV s^{-1}. (b) CV curves of $Ni(OH)_2$/TiN NTA, $Co(OH)_2$/TiN NTA, and $Ni_xCo_{2x}(OH)_{6x}$/TiN NTA at a scan rate of 5 mV s^{-1}.

hydroxides. All the diffraction peaks are weak and broad, indicating the low crystallinity, which can be indexed to $Ni(OH)_2$ (JCPDF: 14-0117) and $Co(OH)_2$ (JCPDF: 02-0925). These Ni−Co hydroxides change into $NiCo_2O_4$ (Figure S3) after calcination, which indicates the molar ratio of Ni and Co in the hydroxides is 1:2. X-ray photoelectron spectroscopy (XPS) results of $Ni_xCo_{2x}(OH)_{6x}$/TiN NTA are presented in Figure 2b−d. The O 1s spectrum (Figure 2b) shows three oxygen contributions: O1 at 531.2 eV is nickel−oxygen bonds and O2 at 532.1 eV is cobalt−oxygen bonds.[28,38] The component O3 at 533.9 eV can be attributed to physi- and chemisorbed water.[28] In the Ni 2p XPS spectrum, the main $2p_{3/2}$ peak is fitted with characteristic Ni^{2+} with minor oxidation to Ni^{3+} and two shakeup satellites (denoted as "Sat."). [39] The Co 2p spectrum is fitted with Co^{2+} and two shakeup satellites.[14] The ratio of Ni/Co calculated from the XPS result is about 1:1.9, which corresponds to the XRD result of Ni−Co hydroxides after calcination.

Electrochemical Characterization. For electrochemical investigation, we chose an electrolyte mixture (Figure S4) to optimize the capacitance of $Ni_xCo_{2x}(OH)_{6x}$ under a stable potential window. The cyclic voltammetry (CV) performance of TiN NTA before and after the deposition of $Ni_xCo_{2x}(OH)_{6x}$ at a scan rate of 100 mV s^{-1} is shown in Figure 3a. The CV curve of TiN NTA clearly shows an ideal rectangular shape (also as shown in Figure S5, even at a fast scan rate of 2.0 V s^{-1}). Apparently, after the deposition of $Ni_xCo_{2x}(OH)_{6x}$, a greatly enlarged CV curve with a pair of redox peaks is observed, which can be attributed to the reversible Faradaic redox reactions of $Ni_xCo_{2x}(OH)_{6x}$ materials and the double layer capacitance provided by reversible adsorption of electrolyte ions onto the surface of the active materials. In this case, the TiN NTA serves as a

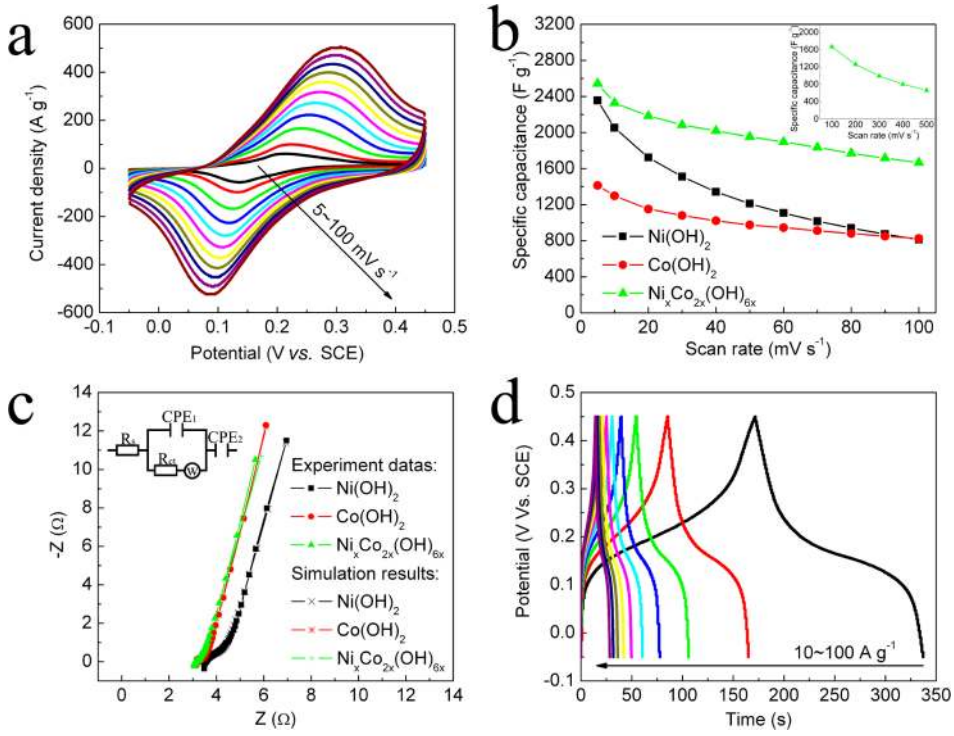

Figure 4. (a) CV curves of a $Ni_xCo_{2x}(OH)_{6x}$/TiN NTA electrode at different scan rates ranging from 5 to 100 mV s^{-1}. (b) Corresponding C_s as a function of scan rates obtained from $Ni(OH)_2$, $Co(OH)_2$, and $Ni_xCo_{2x}(OH)_{6x}$. (c) EIS of $Ni(OH)_2$/TiN NTA, $Co(OH)_2$/TiN NTA, and $Ni_xCo_{2x}(OH)_{6x}$/TiN NTA,. (d) Constant current charge/discharge curves of $Ni_xCo_{2x}(OH)_{6x}$/TiN NTA at various current densities (10−100 A g^{-1}).

nanostructured current collector, playing an important role in the rate capability but with an insignificant capacitance contribution (further discussed below).

CV tests of $Ni(OH)_2$ and $Co(OH)_2$ electrodes are carried out at a scan rate of 5 mV s^{-1} as a fair comparison. As illustrated in Figure 3b, the peaks of the $Ni_xCo_{2x}(OH)_{6x}$ curve are between that of $Co(OH)_2$ and $Ni(OH)_2$, which are near 0.2 and 0.15 V, related to a mixed reaction of 1 and 2.[16,21]

$$Co(OH)_2 + OH^- \leftrightarrow CoOOH + H_2O + e^- \quad (1)$$

$$Ni(OH)_2 + OH^- \leftrightarrow NiOOH + H_2O + e^- \quad (2)$$

As shown in Figure 4a, these peaks located within 0.05−0.3 V are clearly observed in all CV curves over the range 5−100 mV s^{-1}. Even at a scan rate of 100 mV s^{-1}, the CV shape has small distortions. This is because TiN NTA provides a conductive framework for fast electron transport and charge separation. Furthermore, TiN NTA on a mesh substrate with a large surface area endows an enhanced contact of $Ni_xCo_{2x}(OH)_{6x}$ with both the electrolyte and current collector, which can further improve the rate capability.

The specific capacitance (C_s) of this electrode can be calculated based on the CV curves, and the results are displayed in Figure 4b. As a fair comparison, the C_s of $Ni(OH)_2$ and $Co(OH)_2$ calculated from Figure S6 are also shown in Figure 4b. Obviously, with an increasing scan rate from 5 to 100 mV s^{-1}, the C_s of $Ni(OH)_2$ drops quickly (2400 F g^{-1} at 5 mV s^{-1}, 800 F g^{-1} at 100 mV s^{-1}) even when deposited in TiN NTA, which demonstrates that the poor intrinsic conductivity of $Ni(OH)_2$ limits its electrochemical performance at high scan rates. It is worth noting that 2400 F g^{-1} is higher than the theoretical capacitance of $Ni(OH)_2$ (2082 F g^{-1} within 0.5 V, according to Faraday's law). This further confirms that double-layer capacitance offers a notable contribution to the total capacitance of electrodeposited materials. On the other hand, the rate capability of $Co(OH)_2$ is much better (1400 F g^{-1} at 5 mV s^{-1}, 800 F g^{-1} at 100 mV s^{-1}). Compared with the electrodes discussed above, $Ni_xCo_{2x}(OH)_{6x}$ as a combination of $Ni(OH)_2$ and $Co(OH)_2$ *in situ*, exhibits multiple characteristics with both enhanced capacity and rate performance. The capacitance of $Ni_xCo_{2x}(OH)_{6x}$ is impressive at 1665 F g^{-1} at a scan rate of 100 mV s^{-1} (equal to 0.18 F cm^{-2}, as shown in Figure S7), which is higher than previously reported Ni and Co hydroxides.[40−43] Even under a very high rate of 500 mV s^{-1}, the $Ni_xCo_{2x}(OH)_{6x}$ electrode still reveals a quite considerable capacitance of 660 F g^{-1} (inset of Figure 4b).

To confirm these results, electrochemical impedance spectroscopy (EIS) of $Ni(OH)_2$, $Co(OH)_2$, and $Ni_xCo_{2x}(OH)_{6x}$ electrodes are measured at a potential of 0.2 V, applying 5 mV ac voltage in the frequency range from 100 kHz to 1 Hz, respectively. As shown in Figure 4c, all the impedance spectra are composed of one semicircle at high frequency and a linear part at

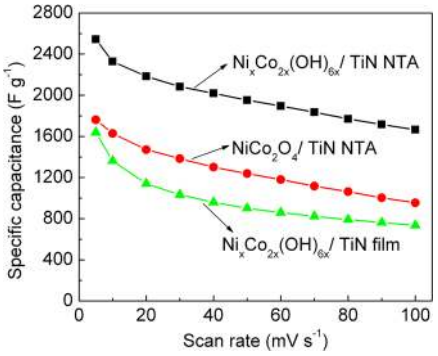

Figure 5. Corresponding C_s as a function of scan rates obtained from $Ni_xCo_{2x}(OH)_{6x}$/TiN NTA, $NiCo_2O_4$/TiN NTA, and $Ni_xCo_{2x}(OH)_{6x}$/TiN film.

low frequency, which illustrates typical capacitor behavior. The internal resistances (R_s) of these electrodes are around 3 Ω. Nevertheless, the electrode R_s of $Co(OH)_2$ and $Ni_xCo_{2x}(OH)_{6x}$ are lower compared to that of $Ni(OH)_2$. This phenomenon contributes to the better intrinsic conductivity of $Co(OH)_2$, in accord with the CV results discussed above. Furthermore, the impedance data are stimulated by an equivalent circuit (inset of Figure 4c), and the simulation results are shown in Table S1. The charge transfer resistance (R_{ct}) of $Ni_xCo_{2x}(OH)_{6x}$/TiN NTA (0.386 Ω) is smaller than that of $Ni(OH)_2$/TiN NTA (0.985 Ω) and $Co(OH)_2$/TiN NTA (0.494 Ω). This result also demonstrates that $Ni_xCo_{2x}(OH)_{6x}$/TiN NTA is a favorable electrode with enhanced electronic conductivity.

In addition, galvanostatic charge−discharge are carried out between −0.05 and 0.45 V at different current densities (10−100 A g^{-1}). As shown in Figure 4d, the potential−time curves at all current densities are almost symmetric, which indicates a high Coulombic efficiency (over 97.5%) because of the highly reversible redox reactions of the $Ni_xCo_{2x}(OH)_{6x}$/TiN NTA electrode on the charge−discharge process. About 84.7% of the C_s is retained when the charge−discharge rate increases from 10 A g^{-1} to 100 A g^{-1}. This also suggests a good rate capability.

TiN NTA current collector plays an important role in the property of the electrode. To evaluate the effect of the current collector, we deposited $Ni_xCo_{2x}(OH)_{6x}$ on TiN NTA and a TiN film mesh substrate (Figure S8), respectively. In Figure 5, $Ni_xCo_{2x}(OH)_{6x}$ on TiN NTA exhibits a much higher capacitance, which is mainly due to the large surface area of NTA, which facilitates contact with $Ni_xCo_{2x}(OH)_{6x}$ and further improves the utilization of $Ni_xCo_{2x}(OH)_{6x}$ during Faradaic reactions. In a further investigation, $NiCo_2O_4$/TiN NTA is prepared

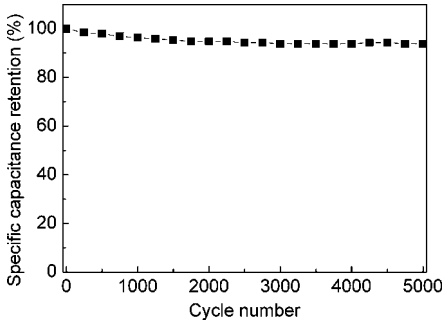

Figure 6. C_s of the $Ni_xCo_{2x}(OH)_{6x}$/TiN NTA electrode as a function of cycle numbers at a scan rate of 100 mV s^{-1}.

by calcination for comparison (Figure S9). Figure 5 also illustrates that the $Ni_xCo_{2x}(OH)_{6x}$/TiN NTA represent a notable enhancement on both capacity and rate performance over $NiCo_2O_4$/TiN NTA. We attribute these improvements to two main factors. First, the valence state of Ni and Co in $Ni_xCo_{2x}(OH)_{6x}$ are both +2 charge, while $NiCo_2O_4$ also contains Ni^{3+} and Co^{3+}.[44,45] Therefore, $Ni_xCo_{2x}(OH)_{6x}$ possesses a higher theoretical C_s according to eqs 1 and 2. Second, the low-crystallinity $Ni_xCo_{2x}(OH)_{6x}$ possesses a high surface area and endows it with more active centers, which will ensure efficient redox reactions and fast ion transport.

Furthermore, cycling performance of the Ni_xCo_{2x}-$(OH)_{6x}$/TiN NTA electrode is evaluated by CV tests at a scan rate of 100 mV s^{-1} for 5000 cycles. As shown in Figure 6, there is about 6.25% C_s loss after 5000 cycles. TiN NTA is an effective stabilizer to support Ni_xCo_{2x}-$(OH)_{6x}$, avoiding collapse of active material during a long cycle. This demonstrates that the $Ni_xCo_{2x}(OH)_{6x}$/TiN NTA electrode is a potential candidate for supercapacitors.

CONCLUSIONS

In summary, we adopted a facile co-electrodeposition to construct a self-standing $Ni_xCo_{2x}(OH)_{6x}$/TiN NTA monolithic electrode. The as-prepared electrode delivers a high C_s of 2543 F g^{-1} at 5 mV s^{-1} and a good rate performance of 660 F g^{-1} even at 500 mV s^{-1}. TiN NTA is important for the enhanced rate performance of our electrode, which provides a large surface area and fast electron transport. The support of TiN NTA also stabilizes the active materials. $Ni_xCo_{2x}(OH)_{6x}$/TiN NTA shows good long-term cycling performance (about 6.25% C_s loss for 5000 cycles). Furthermore, the $Ni_xCo_{2x}(OH)_{6x}$/TiN NTA electrode exhibits much more valuable electrochemical performance than $NiCo_2O_4$/TiN NTA. Our work confirms that the $Ni_xCo_{2x}(OH)_{6x}$/TiN NTA electrode has potential use as a high-performance supercapacitor.

EXPERIMENTAL SECTION

Preparation of TiN NTA. All the chemicals were used as received without further purification. The Ti mesh substrate was anodized in a two-electrode cell (0.1 wt % NH_4F/ethylene glycol as electrolyte, Pt as counter electrode) to obtain the precursor of TiN NTA at 60 V under atmosphere for 7 h. The precursor was

cleaned with ethyl alcohol three times, and then calcined in a tube furnace at 800 °C under ammonia for 1 h. After cooling, TiN NTA was finally obtained. TiN thin films were obtained by directly annealing the Ti mesh substrates under ammonia at 800 °C for 1 h.

Preparation of $Ni_xCo_{2x}(OH)_{6x}$/TiN NTA Electrode. In a typical process, 2 mmol of $Ni(NO_3)_2 \cdot 6H_2O$ and 4 mmol of $Co(NO_3)_2 \cdot 6H_2O$ were dissolved into 40 mL of deionized water to obtain a light pink liquid. Then the co-electrodeposition was conducted at room temperature by a CHI 440A electrochemical workstation with platinum as the counter electrode, a saturated calomel electrode (SCE) as the reference electrode, and TiN NTA as the working electrode. After the co-electrodeposition with a potential at −1.0 V (vs SCE) for 10 s, the sample was carefully washed several times with deionized water. Then the sample was put into a vacuum oven at 120 °C for 8 h. For comparison, $Ni(OH)_2$/TiN NTA and $Co(OH)_2$/TiN NTA were obtained by the same procedure, respectively. The $Ni_xCo_{2x}(OH)_{6x}$/TiN thin film was prepared by co-electrodeposition on the TiN thin films (mesh substrate).

Characterization. In order to reduce the impact of TiN NTA, we deposited $Ni_xCo_{2x}(OH)_{6x}$, $Ni(OH)_2$, and $Co(OH)_2$ on stainless steel, which was easily scratched for X-ray diffraction (XRD) analysis. XRD patterns were recorded with a Bruker-AXS Micro diffractometer (D8 Advance) using Cu Ka radiation (λ =1.5406 Å) from 5° to 95° at a scanning speed of 3° min^{-1}. Morphological information was attained from field emission scanning electron microscopy (Hitachi S-4800). Scanning transmission electron microscope (STEM) and energy dispersive X-ray spectroscopy elemental mapping were obtained from Tecnai F20. X-ray photoelectron spectroscopy was carried out by an ESCALab220i-XL electron spectrometer using Al Kα radiation.

Electrochemical Tests. Electrochemical measurements were carried out by a CHI 440A instrument. The three-electrode system includes SCE as the reference electrode, platinum as the counter electrode, and $Ni_xCo_{2x}(OH)_{6x}$/TiN NTA as the working electrode. In order to obtain a moderate electrolyte with high ionic concentration, we used a 0.1 M KOH and 1.9 M KCl mixture as the electrolyte. At room temperature, cyclic voltammetry was carried out at various scan rates (2−500 mV s^{-1}). Galvanostatic charge/discharge was also carried out at different current densities (10−100 A g^{-1}). Electrochemical impedance spectroscopy was tested by a Zahner Zennium electrochemical workstation (Germany).

The specific capacitance (C_s) of $Ni_xCo_{2x}(OH)_{6x}$ is calculated from the CV curves based on the following equation:

$$C_{Ni_xCo_{2x}(OH)_{6x}} = \frac{Q_{Ni_xCo_{2x}(OH)_{6x}/TiNNTA} - Q_{TiNNTA}}{\Delta V \times m_{Ni_xCo_{2x}(OH)_{6x}}} \quad (3)$$

where C (F g^{-1}) is the C_s, Q (C) is the average charge during the charging and discharging process, ΔV (V) is the potential range, and m (g) is mass of $Ni_xCo_{2x}(OH)_{6x}$ calculated from the charge passed for the deposition.

Conflict of Interest: The authors declare no competing financial interest.

Supporting Information Available: Macroscopic SEM image of TiN NTA, SEM image of $Ni_xCo_{2x}(OH)_{6x}$/TiN film, XRD of $NiCo_2O_4$, CV results, simulation of EIS data. This material is available free of charge *via* the Internet at http://pubs.acs.org.

Acknowledgment. This work was supported by the Key Research Program of the Chinese Academy of Sciences (Grant No. KGZD-EW-202-2), National Natural Science Foundation of China (Grant No. 21275151, 21271180), Doctoral Fund of Shandong Province (BS2012NJ011), and the Key Technology Research Projects of Qingdao (No. 12-4-1-24-gx).

REFERENCES AND NOTES

1. Wang, G.; Zhang, L.; Zhang, J. A Review of Electrode Materials for Electrochemical Supercapacitors. *Chem. Soc. Rev.* **2012**, *41*, 797–828.
2. Zhu, Y.; Murali, S.; Stoller, M. D.; Ganesh, K. J.; Cai, W.; Ferreira, P. J.; Pirkle, A.; Wallace, R. M.; Cychosz, K. A.; Thommes, M.; *et al*. Carbon-Based Supercapacitors Produced by Activation of Graphene. *Science* **2011**, *332*, 1537–1541.
3. Hahm, M. G.; Leela Mohana Reddy, A.; Cole, D. P.; Rivera, M.; Vento, J. A.; Nam, J.; Jung, H. Y.; Kim, Y. L.; Narayanan, N. T.; Hashim, D. P.; *et al*. Carbon Nanotube-Nanocup Hybrid Structures for High Power Supercapacitor Applications. *Nano Lett.* **2012**, *12*, 5616–5621.
4. Guo, C. X.; Li, C. M. A Self-Assembled Hierarchical Nanostructure Comprising Carbon Spheres and Graphene Nanosheets for Enhanced Supercapacitor Performance. *Energy Environ. Sci.* **2011**, *4*, 4504–4507.
5. Chen, Z.; Wen, J.; Yan, C.; Rice, L.; Sohn, H.; Shen, M.; Cai, M.; Dunn, B.; Lu, Y. High-Performance Supercapacitors Based on Hierarchically Porous Graphite Particles. *Adv. Energy Mater.* **2011**, *1*, 551–556.
6. Yan, J. A.; Khoo, E.; Sumboja, A.; Lee, P. S. Facile Coating of Manganese Oxide on Tin Oxide Nanowires with High-Performance Capacitive Behavior. *ACS Nano* **2010**, *4*, 4247–4255.
7. Lu, X.; Yu, M.; Wang, G.; Zhai, T.; Xie, S.; Ling, Y.; Tong, Y.; Li, Y. H-TiO_2@MnO_2//H-TiO_2@C Core-Shell Nanowires for High Performance and Flexible Asymmetric Supercapacitors. *Adv. Mater.* **2013**, *25*, 267–272.
8. Wei, W.; Cui, X.; Chen, W.; Ivey, D. G. Manganese Oxide-Based Materials as Electrochemical Supercapacitor Electrodes. *Chem. Soc. Rev.* **2011**, *40*, 1697–1721.
9. Lu, Q.; Lattanzi, M. W.; Chen, Y.; Kou, X.; Li, W.; Fan, X.; Unruh, K. M.; Chen, J. G.; Xiao, J. Q. Supercapacitor Electrodes with High-Energy and Power Densities Prepared from Monolithic NiO/Ni Nanocomposites. *Angew. Chem., Int. Ed.* **2011**, *50*, 6847–6850.
10. Tang, Z.; Tang, C. H.; Gong, H. A High Energy Density Asymmetric Supercapacitor from Nano-Architectured $Ni(OH)_2$/Carbon Nanotube Electrodes. *Adv. Funct. Mater.* **2012**, *22*, 1272–1278.
11. Yuan, Y. F.; Xia, X. H.; Wu, J. B.; Yang, J. L.; Chen, Y. B.; Guo, S. Y. Nickel Foam-Supported Porous $Ni(OH)_2$/NiOOH Composite Film as Advanced Pseudocapacitor Material. *Electrochim. Acta* **2011**, *56*, 2627–2632.
12. Li, X.; Xiong, S.; Li, J.; Bai, J.; Qian, Y. Mesoporous NiO Ultrathin Nanowire Networks Topotactically Transformed from α-$Ni(OH)_2$ Hierarchical Microspheres and Their Superior Electrochemical Capacitance Properties and Excellent Capability for Water Treatment. *J. Mater. Chem.* **2012**, *22*, 14276–14283.
13. Yuan, C.; Hou, L.; Shen, L.; Li, D.; Zhang, F.; Fan, C.; Li, J.; Zhang, X. A Novel Method to Synthesize Whisker-like $Co(OH)_2$ and Its Electrochemical Properties as an Electrochemical Capacitor Electrode. *Electrochim. Acta* **2010**, *56*, 115–121.
14. Chang, J. K.; Wu, C. M.; Sun, I. W. Nano-Architectured $Co(OH)_2$ Electrodes Constructed Using an Easily-Manipulated Electrochemical Protocol for High-Performance Energy Storage Applications. *J. Mater. Chem.* **2010**, *20*, 3729–3735.
15. Wang, H. L.; Casalongue, H. S.; Liang, Y. Y.; Dai, H. J. $Ni(OH)_2$ Nanoplates Grown on Graphene as Advanced Electrochemical Pseudocapacitor Materials. *J. Am. Chem. Soc.* **2010**, *132*, 7472–7477.
16. Li, J.; Yang, M.; Wei, J.; Zhou, Z. Preparation and Electrochemical Performances of Doughnut-like $Ni(OH)_2$-$Co(OH)_2$ Composites as Pseudocapacitor Materials. *Nanoscale* **2012**, *4*, 4498–4503.
17. Wu, H. Y.; Wang, H. W. Electrochemical Synthesis of Nickel Oxide Nanoparticulate Films on Nickel Foils for High-Performance Electrode Materials of Supercapacitors. *Int. J. Electrochem. Sci.* **2012**, *7*, 4405–4417.
18. Yuan, C.; Zhang, X.; Hou, L.; Shen, L.; Li, D.; Zhang, F.; Fan, C.; Li, J. Lysine-Assisted Hydrothermal Synthesis of Urchin-like Ordered Arrays of Mesoporous $Co(OH)_2$ Nanowires and Their Application in Electrochemical Capacitors. *J. Mater. Chem.* **2010**, *20*, 10809–10816.
19. Zhou, W. J.; Xu, M. W.; Zhao, D. D.; Xu, C. L.; Li, H. L. Electrodeposition and Characterization of Ordered

Mesoporous Cobalt Hydroxide Films on Different Substrates for Supercapacitors. *Microporous Mesoporous Mater.* **2009**, *117*, 55–60.
20. Chang, J.; Sun, J.; Xu, C.; Xu, H.; Gao, L. Template-Free Approach to Synthesize Hierarchical Porous Nickel Cobalt Oxides for Supercapacitors. *Nanoscale* **2012**, *4*, 6786–6791.
21. Tao, Y.; Zaijun, L.; Ruiyi, L.; Qi, N.; Hui, K.; Yulian, N.; Junkang, L. Nickel−Cobalt Double Hydroxides Microspheres with Hollow Interior and Hedgehog-like Exterior Structures for Supercapacitors. *J. Mater. Chem.* **2012**, *22*, 23587–23592.
22. Guan, C.; Liu, J.; Cheng, C.; Li, H.; Li, X.; Zhou, W.; Zhang, H.; Fan, H. J. Hybrid Structure of Cobalt Monoxide Nanowire @ Nickel Hydroxidenitrate Nanoflake Aligned on Nickel Foam for High-Rate Supercapacitor. *Energy Environ. Sci.* **2011**, *4*, 4496–4499.
23. Hu, C. C.; Chen, J. C.; Chang, K. H. Cathodic Deposition of $Ni(OH)_2$ and $Co(OH)_2$ for Asymmetric Supercapacitors: Importance of the Electrochemical Reversibility of Redox Couples. *J. Power Sources* **2013**, *221*, 128–133.
24. Yang, F.; Yao, J.; Liu, F.; He, H.; Zhou, M.; Xiao, P.; Zhang, Y. Ni−Co Oxides Nanowire Arrays Grown on Ordered TiO_2 Nanotubes with High Performance in Supercapacitors. *J. Mater. Chem. A* **2013**, *1*, 594–601.
25. Jiang, J.; Li, Y.; Liu, J.; Huang, X.; Yuan, C.; Lou, X. W. Recent Advances in Metal Oxide-Based Electrode Architecture Design for Electrochemical Energy Storage. *Adv. Mater.* **2012**, *24*, 5166–5180.
26. Zhang, G. Q.; Wu, H. B.; Hoster, H. E.; Chan-Park, M. B.; Lou, X. W. Single-Crystalline $NiCo_2O_4$ Nanoneedle Arrays Grown on Conductive Substrates as Binder-Free Electrodes for High-Performance Supercapacitors. *Energy Environ. Sci.* **2012**, *5*, 9453–9456.
27. Yu, L.; Zhang, G.; Yuan, C.; Lou, X. W. Hierarchical $NiCo_2O_4$@MnO_2 Core-Shell Heterostructured Nanowire Arrays on Ni Foam as High-Performance Supercapacitor Electrodes. *Chem. Commun.* **2013**, *49*, 137–139.
28. Yuan, C.; Li, J.; Hou, L.; Zhang, X.; Shen, L.; Lou, X. W. D. Ultrathin Mesoporous $NiCo_2O_4$ Nanosheets Supported on Ni Foam as Advanced Electrodes for Supercapacitors. *Adv. Funct. Mater.* **2012**, *22*, 4592–4597.
29. Zhang, G.; Lou, X. W. General Solution Growth of Mesoporous $NiCo_2O_4$ Nanosheets on Various Conductive Substrates as High-Performance Electrodes for Supercapacitors. *Adv. Mater.* **2013**, *25*, 976–979.
30. Choi, D.; Kumta, P. N. Nanocrystalline TiN Derived by a Two-Step Halide Approach for Electrochemical Capacitors. *J. Electrochem. Soc.* **2006**, *153*, A2298–A2303.
31. Bang, J. H.; Suslick, K. S. Dual Templating Synthesis of Mesoporous Titanium Nitride Microspheres. *Adv. Mater.* **2009**, *21*, 3186–3190.
32. Chien, H. C.; Cheng, W. Y.; Wang, Y. H.; Lu, S. Y. Ultrahigh Specific Capacitances for Supercapacitors Achieved by Nickel Cobaltite/Carbon Aerogel Composites. *Adv. Funct. Mater.* **2012**, *22*, 5038–5043.
33. Jiang, H.; Ma, J.; Li, C. Hierarchical Porous $NiCo_2O_4$ Nanowires for High-Rate Supercapacitors. *Chem. Commun.* **2012**, *48*, 4465–4467.
34. Wang, H. W.; Hu, Z. A.; Chang, Y. Q.; Chen, Y. L.; Wu, H. Y.; Zhang, Z. Y.; Yang, Y. Y. Design and Synthesis of $NiCo_2O_4$-Reduced Graphene Oxide Composites for High Performance Supercapacitors. *J. Mater. Chem.* **2011**, *21*, 10504–10511.
35. Xiao, J.; Yang, S. Sequential Crystallization of Sea Urchin-like Bimetallic (Ni, Co) Carbonate Hydroxide and Its Morphology Conserved Conversion to Porous $NiCo_2O_4$ Spinel for Pseudocapacitors. *RSC Adv.* **2011**, *1*, 588–595.
36. Dong, S.; Chen, X.; Wang, S.; Gu, L.; Zhang, L.; Wang, X.; Zhou, X.; Liu, Z.; Han, P.; Duan, Y.; *et al.* 1D Coaxial Platinum/Titanium Nitride Nanotube Arrays with Enhanced Electrocatalytic Activity for the Oxygen Reduction Reaction: Towards Li-Air Batteries. *ChemSusChem* **2012**, *5*, 1712–1715.
37. Dong, S.; Chen, X.; Gu, L.; Zhou, X.; Li, L.; Liu, Z.; Han, P.; Xu, H.; Yao, J.; Wang, H.; *et al.* One Dimensional MnO_2/Titanium Nitride Nanotube Coaxial Arrays for High Performance Electrochemical Capacitive Energy Storage. *Energy Environ. Sci.* **2011**, *4*, 3502–3508.
38. Fihri, A.; Sougrat, R.; Rakhi, R. B.; Rahal, R.; Cha, D.; Hedhili, M. N.; Bouhrara, M.; Alshareef, H. N.; Polshettiwar, V. Nanoroses of Nickel Oxides: Synthesis, Electron Tomography Study, and Application in CO Oxidation and Energy Storage. *ChemSusChem* **2012**, *5*, 1241–1248.
39. Cui, B.; Lin, H.; Li, Y. Z.; Li, J. B.; Sun, P.; Zhao, X. C.; Liu, C. J. Photophysical and Photocatalytic Properties of Core-Ring Structured $NiCo_2O_4$ Nanoplatelets. *J. Phys. Chem. C* **2009**, *113*, 14083–14087.
40. Lee, J. W.; Ahn, T.; Soundararajan, D.; Ko, J. M.; Kim, J. D. Non-Aqueous Approach to the Preparation of Reduced Graphene Oxide/alpha-$Ni(OH)_2$ Hybrid Composites and Their High Capacitance Behavior. *Chem. Commun.* **2011**, *47*, 6305–6307.
41. Jiang, H.; Zhao, T.; Li, C.; Ma, J. Hierarchical Self-Assembly of Ultrathin Nickel Hydroxide Nanoflakes for High-Performance Supercapacitors. *J. Mater. Chem.* **2011**, *21*, 3818–3823.
42. Liang, Y. Y.; Cao, L.; Kong, L. B.; Li, H. L. Synthesis of $Co(OH)_2$/USY Composite and Its Application for Electrochemical Supercapacitors. *J. Power Sources* **2004**, *136*, 197–200.
43. Kong, L. B.; Lang, J. W.; Liu, M.; Luo, Y. C.; Kang, L. Facile Approach to Prepare Loose-Packed Cobalt Hydroxide Nano-Flakes Materials for Electrochemical Capacitors. *J. Power Sources* **2009**, *194*, 1194–1201.
44. Kim, J. G.; Pugmire, D. L.; Battaglia, D.; Langell, M. A. Analysis of the $NiCo_2O_4$ Spinel Surface with Auger and X-Ray Photoelectron Spectroscopy. *Appl. Surf. Sci.* **2000**, *165*, 70–84.
45. Marco, J. Characterization of the Nickel Cobaltite, $NiCo_2O_4$, Prepared by Several Methods: An XRD, XANES, EXAFS, and XPS Study. *J. Solid State Chem.* **2000**, *153*, 74–81.